Eur. J. Mineral.
2015, **27**, 405–415
Published online 10 February 2015

Mambertiite, $BiMo^{5+}_{2.80}O_8(OH)$, a new mineral from Su Seinargiu, Sardinia, Italy: occurrence, crystal structure, and relationships with gelosaite

PAOLO ORLANDI[1], CRISTIAN BIAGIONI[1,*], MARCO PASERO[1], FRANCESCO DEMARTIN[2], ITALO CAMPOSTRINI[2] and STEFANO MERLINO[1]

[1] Dipartimento di Scienze della Terra, Università di Pisa, Via S. Maria 53, 56126 Pisa, Italy
*Corresponding author, e-mail: biagioni@dst.unipi.it
[2] Dipartimento di Chimica, Università degli Studi di Milano, Via Golgi 19, 20133 Milano, Italy

Abstract: Mambertiite, $BiMo^{5+}_{2.80}O_8(OH)$, is a new mineral identified in small vugs of quartz veins from Su Seinargiu, Sarroch, Cagliari, Sardinia, Italy. It occurs as pale yellow {001} tabular crystals, up to 1 mm in length and few μm thick, with adamantine lustre. Mambertiite is brittle, with a conchoidal fracture. It is associated with ferrimolybdite, muscovite, quartz, sardignaite, and wulfenite. Electron microprobe data (wt% – mean of 12 spot analyses) are: Mo_2O_5 59.59, Bi_2O_3 36.96, WO_3 2.03, H_2O_{calc} 1.48, sum 100.06. On the basis of 9 O atoms per formula unit, the empirical formula is $Bi_{0.99}(Mo^{5+}_{2.74}W_{0.05})_{\Sigma 2.79}O_{7.97}(OH)_{1.03}$. Infrared spectra showed absorption bands consistent with the occurrence of OH^- groups. Mambertiite is triclinic, space group $P\overline{1}$, with $a = 5.854(2)$, $b = 9.050(3)$, $c = 7.637(3)$ Å, $\alpha = 112.85(1)$, $\beta = 102.58(1)$, $\gamma = 90.04(1)°$, $V = 362.3(2)$ Å^3, $Z = 2$. The crystal structure of mambertiite was solved and refined down to $R_1 = 0.050$ on the basis of 2019 observed [$F_o > 4\sigma(F_o)$] reflections. It is composed by eight-fold coordinated Bi-centred polyhedra and five independent Mo-centred octahedra. Among the latter, two are completely occupied by molybdenum, whereas the remaining three are only partially occupied. Two kinds of $(10\overline{1})$ layers occur in mambertiite, alternating along $[10\overline{1}]^*$: one is composed by Bi-centered polyhedra and the two partially occupied Mo4 and Mo5 sites, whereas the other is composed by the zigzag chains, running along **c**, formed by the fully occupied Mo1 and Mo2 sites, and the partially occupied Mo3 site. Mambertiite is structurally related to gelosaite, $BiMo^{6+}_2O_7(OH) \cdot H_2O$; their relationships can be conveniently described through the OD theory. Mambertiite is the fourth known mineral with Bi and Mo as essential components. Its name honours the Italian mineral collector Marzio Mamberti (b. 1959) for his contribution to the knowledge of the Sardinian mineralogy. The mineral and its name have been approved by the IMA CNMNC (No. 2013–098).

Key-words: mambertiite; new mineral; bismuth; molybdenum; oxide; crystal structure; Su Seinargiu; Sardinia; Italy.

1. Introduction

In the past, Sardinia Island (Italy) was the most important Italian mining region. Notwithstanding the large variety of ore deposits occurring in this area, a relatively small number of mineral species have their type locality in Sardinia (Table 1). One of the most important occurrences is the Mo-Bi mineralization of Su Seinargiu, Sarroch, Cagliari. Indeed, six new mineral species have been recently discovered there. All these phases are the product of the alteration of the primary molybdenite ± bismuthinite ± bismuth assemblage, with the formation of a series of bismuth and molybdenum secondary minerals: bismite, bismoclite, bismutite, cannonite, ferrimolybdite, ichnusaite, nuragheite, tancaite-(Ce), wulfenite, and a mendozavilite-group mineral (Orlandi *et al.*, 2013, 2014, 2015). In addition, four Bi-Mo species have been identified: gelosaite, koechlinite, sardignaite (Orlandi *et al.*, 2013), and the new mineral mambertiite herewith described.

This mineral species and its name have been approved by the IMA CNMNC (No. 2013–098). The holotype specimen of mambertiite is deposited in the mineralogical collection of the Museo di Storia Naturale, Università di Pisa, via Roma 79, Calci, Pisa, Italy, under catalogue number 19682. The name honours the Italian mineral collector Marzio Mamberti (b. 1959) for his contribution to the study of the Sardinian mineralogy and, in particular, of the Mo-Bi mineralization of Su Seinargiu. Marzio Mamberti provided us with the first specimen of sardignaite (Orlandi *et al.*, 2010) and additional samples of gelosaite (Orlandi *et al.*, 2011), ichnusaite (Orlandi *et al.*, 2014), and nuragheite (Orlandi *et al.*, 2015), useful for their full characterization.

0935-1221/15/0027-2434 $ 4.95
DOI: 10.1127/ejm/2015/0027-2434

Table 1. Mineral species first found in Sardinia. In bold, the new minerals from Su Seinargiu.

Mineral species	Chemical formula	Type locality	Ref.
Barrerite	$(Na,K,Ca_{0.5})_2[Al_2Si_7O_{18}] \cdot 7H_2O$	Pula	[1]
Gelosaite	$BiMo^{6+}{}_2O_7(OH) \cdot H_2O$	Su Seinargiu	[2]
Ichnusaite	$Th(MoO_4)_2 \cdot 3H_2O$	Su Seinargiu	[3]
Mambertiite	$BiMo^{5+}{}_{2.80}O_8(OH)$	Su Seinargiu	[4]
Monteponite	CdO	Monteponi	[5]
Nuragheite	$Th(MoO_4)_2 \cdot H_2O$	Su Seinargiu	[6]
Orlandiite	$Pb_{10}(SeO_4)O_7Cl \cdot H_2O$	Baccu Locci	[7]
Rosasite	$(Cu,Zn)_2(CO_3)(OH)_2$	Rosas	[8]
Sabelliite	$(Cu,Zn)Zn(AsO_4,SbO_4)(OH)_3$	Is Murvonis	[9]
Sardignaite	$BiMo_2O_7(OH) \cdot 2H_2O$	Su Seinargiu	[10]
Sarrabusite	$Pb_5CuCl_4(SeO_3)_4$	Baccu Locci	[11]
Stilbite-Na	$(Na,Ca,K)_{6-7}[Al_8Si_{28}O_{72}] \cdot nH_2O$	Pula	[12]
Tancaite-(Ce)	$FeCe(MoO_4)_3 \cdot 3H_2O$	Su Seinargiu	[13]

[1] Passaglia & Pongiluppi (1975); [2] Orlandi *et al.* (2011); [3] Orlandi *et al.* (2014); [4] this work.; [5] Wittich & Neumann (1901); [6] Orlandi *et al.* (2015); [7] Campostrini *et al.* (1999); [8] Lovisato (1908); [9] Olmi *et al.* (1995); [10] Orlandi *et al.* (2010); [11] Gemmi *et al.* (2012); [12] Passaglia *et al.* (1978); [13] Bonaccorsi & Orlandi (2010).

2. Occurrence and mineral description

2.1. Occurrence and physical properties

The geological setting of the Su Seinargiu prospect has been briefly reported in previous papers (e.g., Orlandi *et al.*, 2014 and references therein). The mineralization consists of three vein systems, mainly composed by quartz and molybdenite with minor bismuthinite and bismuth, hosted in leucogranite porphyry, embedded in shales of Ordovician-Silurian age and low metamorphic grade. Owing to the occurrence of more than 50 different mineral phases (Orlandi *et al.*, 2013) and the description of six new minerals (Table 1), represented by molybdenum oxides and molybdates, Su Seinargiu has become a reference locality for the study of secondary molybdenum species.

Mambertiite is very rare and it has been identified so far in only two specimens. It occurs as {001} tabular crystals, up to 1 mm in length and few μm in thickness (Fig. 1), with a pale yellow colour and a white streak. Lustre is adamantine. The mineral is brittle, with a conchoidal fracture and without any evident cleavage.

Owing to the very small amount of available material and its very small size, micro-indentation hardness, density, and optical properties could not be measured. The calculated densities, on the basis of the empirical formula given below and of the ideal formula, are 5.720 and 5.707 g/cm^3, respectively. By using the ideal formula and the calculated density, a mean refractive index of 2.20 was obtained through the Gladstone-Dale relationship (Mandarino, 1979; 1981).

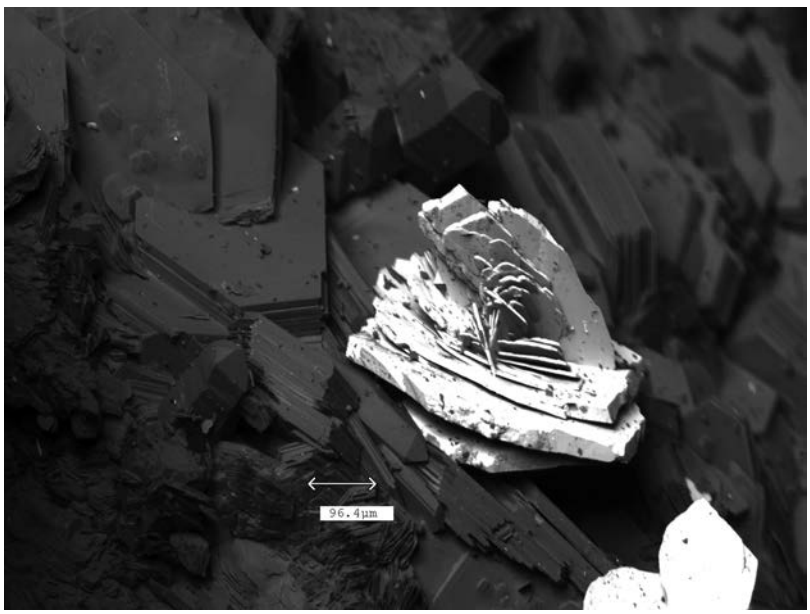

Fig. 1. Back-scattered electron image of an aggregate of {001} tabular crystals of mambertiite, associated with muscovite and quartz.

Mambertiite is associated with ferrimolybdite, muscovite, quartz, sardignaite, and wulfenite in small vugs of the quartz veins. Its crystallization is related to the alteration of the Mo-Bi ore.

2.2. Chemical data and infra-red spectroscopy

Preliminary qualitative chemical analyses were performed using a Philips XL30 scanning electron microscope equipped with an EDAX DX4 system. The only elements with $Z > 9$ detected in mambertiite were Bi, Mo, and minor W.

Electron-microprobe analyses were carried on with an IXRF Sirius SD-10128-LE instrument in energy-dispersive mode. This analytical mode was chosen because the sample was severely damaged by using the wavelength-dispersive mode, even with a large beam diameter. Analytical conditions were: accelerating voltage 20 kV, beam current 10^{-11} A, beam size 2 μm. A well-characterized specimen of gelosaite (yellow crystal from the holotype specimen from Su Seinargiu) was used as standard for Bi and Mo, whereas metallic W was chosen as standard for W. The H_2O content was calculated by stoichiometry from the results of the crystal structure analysis and adjusted in order to obtain a charge-balanced formula. The infra-red spectrum (Fig. 2), recorded on a Jasco IRT-3000 spectrometer using a diamond compression cell, shows a broad band at about 3400 cm^{-1}, consistent with the presence of H_2O or OH^- groups.

Chemical data are given in Table 2. With respect to gelosaite, mambertiite has a significant molybdenum excess, confirmed by the crystal-structure refinement (see below). Molybdenum is given as Mo_2O_5 in order to maintain the electrostatic neutrality that requires its 5+ oxidation state. The empirical formula of mambertiite, based on 9 O atoms per formula unit (*apfu*), is $Bi_{0.99}(Mo^{5+}{}_{2.74}W_{0.05})_{\Sigma 2.79}O_{7.97}(OH)_{1.03}$. Its simplified chemical formula is $BiMo^{5+}{}_{2.80}O_8(OH)$, which requires Mo_2O_5 61.13, Bi_2O_3 37.42, H_2O 1.45, total 100.00 wt%.

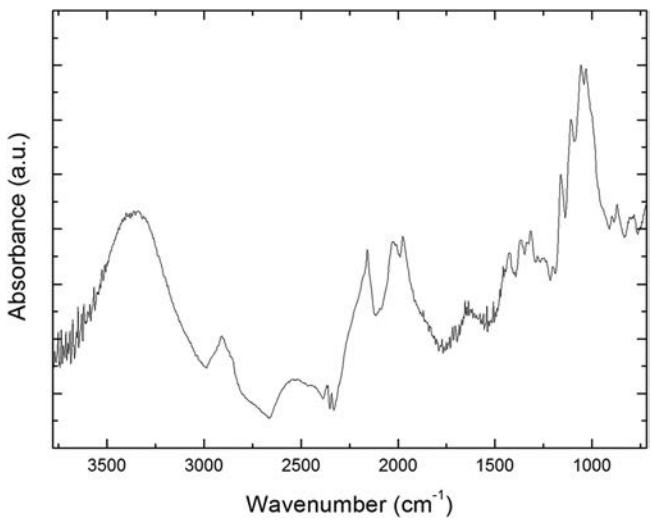

Fig. 2. Infra-red spectrum of mambertiite.

Table 2. Chemical data of mambertiite (as wt% – average of 12 spot analyses). H_2O content was calculated on the basis of stoichiometry.

Oxide	wt%	Range	SD	Probe standard
Mo_2O_5	59.59	56.09–61.03	0.33	gelosaite
Bi_2O_3	36.96	34.69–38.66	0.48	gelosaite
WO_3	2.03	1.60–2.52	0.32	metallic W
H_2O_{calc}	1.48			
Total	100.06			

2.3. Crystallography

The X-ray powder diffraction pattern of mambertiite was obtained using a 114.6 mm diameter Gandolfi camera, with Ni-filtered Cu*K*α radiation. The observed X-ray powder diffraction pattern is compared with the calculated one (obtained using the software Powder Cell; Kraus & Nolze, 1996) in Table 3. Unit-cell parameters, refined using Unit Cell (Holland & Redfern, 1997) on the basis of 22 unequivocally indexed reflections, are $a = 5.825(1)$, $b = 9.174(3)$, $c = 7.702(1)$ Å, $\alpha = 113.63(2)$, $\beta = 102.23(1)$, $\gamma = 90.38(2)°$, $V = 366.6(1)$ Å^3.

Single-crystal X-ray diffraction data were collected using a Bruker Apex II diffractometer equipped with a 2K CCD detector with graphite-monochromatized Mo*K*α radiation. A one-minute frame-time and 0.3° frame-width were used. A total of 3733 reflections were measured; data were integrated and corrected for Lorentz, polarization, and background effects. The absorption ($\mu = 28.92$ mm^{-1}) was corrected using SADABS (Bruker AXS Inc., 2001). Statistical test ($|E^2\text{-}1| = 0.809$) did not indicate unequivocally the centrosymmetric nature of mambertiite. However, the crystal structure solution was tried in the space group $P\bar{1}$. Refined unit-cell parameters are $a = 5.854(2)$, $b = 9.050(3)$, $c = 7.637(3)$ Å, $\alpha = 112.85(1)$, $\beta = 102.58(1)$, $\gamma = 90.04(1)°$, $V = 362.3(2)$ Å^3, $Z = 2$. The a:b:c ratio, using the single-crystal data, is 0.6469:1:0.7776.

The crystal structure was solved through direct methods using Shelxs-97 and refined through Shelxl-97 (Sheldrick, 2008). Scattering curves for neutral atoms were taken from the *International Tables for Crystallography* (Wilson, 1992). After having located the heavier atoms (one Bi and two Mo atoms at Bi, Mo1, and Mo2 sites), the difference-Fourier map showed the presence of three high residuals, interpreted as partially occupied Mo positions. The site occupancies of these three sites were freely refined.

By adding these three atom positions, the R_1 value dropped from 0.177 to 0.121. Through successive difference-Fourier maps, the positions of nine oxygen atoms were located, achieving an isotropic R_1 value of 0.065. After introducing the anisotropic displacement parameters for cations, the R_1 value converged to 0.051. Finally, anisotropic displacement parameters were refined for oxygen atoms (with the exception of O4 and O8 atoms),

Table 3. X-ray powder diffraction data for mambertiite.

I_{obs}	d_{obs}	I_{calc}	d_{calc}	*h k l*	I_{obs}	d_{obs}	I_{calc}	d_{calc}	*h k l*
ms	8.3*	32	8.30	0 1 0	vw	2.628*	7	2.616	2 1 0
w	7.50†				mw	2.504*	36	2.496	2 0 –2
s	**6.80**	7	6.84	0 0 1			5	2.486	−2 1 –1
		48	6.76	0 1 –1	mw	2.468*	9	2.462	0 1 –3
m	5.66*	61	5.69	1 0 0			6	2.457	−2 2 0
s	**4.92***	80	4.91	−1 1 0	w	2.399	12	2.401	1 3 0
m	4.76*	34	4.73	1 1 –1			12	2.389	−1 3 –2
m	4.50*	38	4.498	1 1 0	w	2.281	6	2.313	1 0 –3
w	4.34†				m	2.257	8	2.251	0 4 –1
w	4.06*	5	4.051	−1 1 –1			8	2.246	−1 2 2
w	3.944*	11	3.933	−1 1 1	**ms**	**2.088**	42	2.085	−2 3 0
w	3.803†						42	2.080	2 3 –2
		12	3.577	1 2 –1	vw	2.030*	9	2.026	−2 2 –2
m	3.529*	50	3.516	−1 2 0			7	1.969	2 0 2
m	3.491*	28	3.479	1 1 –2	ms	1.902	18	1.896	3 0 0
vs	**3.417***	100	3.419	0 0 2			13	1.896	2 3 0
		20	3.402	−1 2 –1			13	1.889	−2 3 –2
		13	3.381	0 2 –2			6	1.888	−3 1 0
w	3.300*	16	3.295	1 0 –2	w	1.865*	9	1.863	0 2 –4
m	3.222	38	3.211	1 2 0			8	1.842	−1 3 2
		10	3.211	1 1 1	w	1.832*	8	1.830	1 3 –4
ms	**3.136***	47	3.130	1 2 –2			7	1.825	0 3 2
w	3.055*	9	3.050	0 2 1			7	1.812	0 3 –4
w	2.922*	17	2.909	−1 2 1	w	1.796*	6	1.800	2 1 2
ms	**2.850**	13	2.848	−1 1 –2	w	1.762	6	1.777	3 2 –2
		70	2.844	2 0 0			17	1.756	1 0 –4
s	**2.772**	12	2.794	0 1 2	vw	1.732	9	1.729	1 5 –2
		58	2.768	0 3 0			6	1.729	0 2 3
		9	2.766	−1 1 2	mw	1.693	7	1.707	−1 5 –2
		57	2.753	0 3 –2			16	1.688	−2 3 2
		14	2.725	−1 2 –2			16	1.679	2 3 –4
m	2.674*	38	2.665	1 0 2	m	1.653	14	1.649	1 3 2
							10	1.647	2 0 –4

The d_{hkl} values were calculated on the basis of the unit cell refined by using single-crystal data. Intensities ($I/I_{100} \times 100 > 5$ only) were calculated on the basis of the structural model using Powder Cell (Kraus & Nolze, 1996). Observed intensities were visually estimated: vs = very strong, s = strong, ms = medium-strong, m = medium, mw = medium-weak, w = weak, vw = very weak. The seven strongest reflections are given in bold. Reflections used in the least-squares refinement of unit-cell parameters are indicated by an asterisk. The three unindexed reflections (†) were interpreted as due to admixture phase(s).

converging to a final $R_1 = 0.050$ for 2019 observed [$F_o > 4\sigma(F_o)$] reflections. The highest residuals ($\sim 8\ e^-/\text{Å}^3$) are located around Mo1 and Mo2 sites. These maxima could be related to the low diffraction quality of the studied crystals, characterized by the coexistence of three individuals having different orientations. These individuals are probably related to the {010} twinning law characterizing mambertiite (see § 4.1).

Details of the crystal-structure refinement are given in Table 4, whereas atomic coordinates and displacement parameters are reported in Table 5. Table 6 gives selected bond distances for cation sites. Bond-valence balance, calculated using the parameters given by Krivovichev (2012) and Chen *et al.* (2002) for Bi^{3+}–O and Mo^{5+}–O, respectively, is given in Table 7.

On the basis of the crystal structure refinement and the bond-valence calculation (see § 3.2), the X-ray structural formula of mambertiite can be written as $Bi_{1.00}Mo^{5+}{}_{2.79}O_8(OH)$, in very good agreement with the chemical data. The total site scattering at the Mo sites, *i.e.* 117.6 *epfu* (electron per formula unit), agrees with the value calculated from the chemical formula, *i.e.* 118.8 *epfu.*

3. Crystal-structure description

3.1. General features and cation coordination

The crystal structure of mambertiite is formed by three fully occupied cation sites (Bi, Mo1, and Mo2), three partially occupied cation sites (Mo3, Mo4, and Mo5), and nine anion positions. Neglecting the fractional Mo3, Mo4, and Mo5 sites, Mo1 and Mo2 octahedra form zig-zag chains, running along **b** and connected through edge-sharing (Fig. 3). They are topologically identical to those occurring in gelosaite. Bi dimers occur between these octahedral chains.

The crystal structure can be also described as formed by two kinds of alternating $(10\bar{1})$ layers (Fig. 4a): the first one is composed by the distorted Mo1 and Mo2 octahedra, and

Table 4. Crystal data and summary of parameters describing data collection and refinement for mambertiite.

Crystal data	
Crystal size (mm^3)	$0.025 \times 0.010 \times 0.005$
Cell setting, space group	Triclinic, $P\bar{1}$
a (Å)	5.854(2)
b (Å)	9.050(3)
c (Å)	7.637(3)
α (°)	112.85(1)
β (°)	102.58(1)
γ (°)	90.04(1)
V ($Å^3$)	362.3(2)
Z	2
Data collection and refinement	
Radiation, wavelength (Å)	Mo$K\alpha$, $\lambda = 0.71073$
Temperature (K)	293
$2\theta_{max}$ (°)	62.81
Measured reflections	3733
Unique reflections	2134
Reflections with $F_o > 4\sigma(F_o)$	2019
R_{int}	0.0286
$R\sigma$	0.0331
Range of h, k, l	$-8 \leq h \leq 8, -12 \leq k \leq 12, -10 \leq l \leq 10$
R [$F_o > 4\sigma(F_o)$]	0.0503
R (all data)	0.0527
wR (on F_o^2)	0.1369
Goof	1.089
Number of least-squares parameters	132
Maximum and minimum residual peak (e $Å^{-3}$)	8.11 (at 0.65 Å from Mo1) –2.97 (at 0.68 Å from Bi)

Note: the weighting scheme is defined as $w = 1/[\sigma^2(F_o^2) + (aP)^2 + bP]$, with $P = [2F_c^2 + \mathrm{Max}(F_o^2,0)]/3$: a and b values are 0.0785 and 18.4017.

the partially occupied Mo3 sites (Fig. 4b). Bi polyhedra and the partially occupied Mo4 and Mo5 sites constitute the second kind of layer (Fig. 4c).

The Bi polyhedron can be described as a slightly distorted bicapped trigonal prism. As in gelosaite (Orlandi *et al.*, 2011), the Bi polyhedra form dimeric units by sharing an edge formed by two symmetry related O1 atoms.

The Mo^{5+} is hosted at five octahedral sites. Two of them, Mo1 and Mo2, are fully occupied. They can be described as distorted octahedra, with a short and a long apical bond distance (1.724 and 2.584 Å for Mo1, and 1.711 and 2.544 Å for Mo2). The equatorial bond distances are distorted with two distances ranging from 1.901 and 1.947 Å, whereas the other bond distances are short (1.739 and 1.747 Å for Mo2 and Mo1, respectively) and long (2.127 and 2.141 Å for Mo1 and Mo2, respectively). Such a geometry reminds one of the Mo^{5+} octahedra described in some synthetic compounds (*e.g.*, Ledain *et al.*, 1997a, b), even if the equatorial bonds in mambertiite are unusually distorted. The partially occupied Mo3, Mo4, and Mo5 sites are at about 2.6–2.7 Å apart from the others Mo sites; such distances are not unusual in molybdenum clusters, being observed in synthetic compounds (*e.g.*, Lu *et al.*, 1999) and also in gelosaite (Orlandi *et al.*, 2011). Mo3 is at only 2.677(4) Å from Bi, a distance a little

Table 5. Atomic positions, site occupancies (s.o.f.), and displacement parameters (in $Å^2$) for mambertiite.

Site	s.o.f.	x	y	z	U_{eq}	U_{11}	U_{22}	U_{33}	U_{23}	U_{13}	U_{12}
Bi	$Bi_{1.00}$	0.29747(5)	0.84601(3)	0.28673(4)	0.00935(7)	0.01021(12)	0.00908(11)	0.00967(11)	0.00453(9)	0.00267(9)	0.00010(9)
Mo1	$Mo_{1.00}$	0.7093(1)	0.1217(1)	0.1828(1)	0.00790(13)	0.0056(2)	0.0129(3)	0.0051(2)	0.0039(2)	0.0005(2)	−0.0004(2)
Mo2	$Mo_{1.00}$	0.7074(1)	0.5010(1)	0.1850(1)	0.00842(14)	0.0061(2)	0.0114(3)	0.0056(2)	0.0014(2)	0.0012(2)	−0.0002(2)
Mo3	$Mo_{0.203(3)}$	0.7091(7)	0.8137(8)	0.1833(6)	0.038(2)	0.003(2)	0.086(5)	0.002(2)	−0.008(2)	0.0004(12)	0.006(2)
Mo4	$Mo_{0.300(3)}$	0.2985(4)	0.1806(3)	0.2866(3)	0.0116(6)	0.0089(10)	0.0182(11)	0.0079(8)	0.0048(7)	0.0030(7)	0.0022(8)
Mo5	$Mo_{0.292(2)}$	0.2970(5)	0.5088(4)	0.2861(4)	0.0169(7)	0.0108(11)	0.0320(14)	0.0079(9)	0.0073(9)	0.0038(8)	0.0022(10)
O1	$O_{1.00}$	0.6636(12)	0.9008(7)	0.4606(9)	0.0116(13)	0.016(3)	0.006(2)	0.008(2)	0.003(2)	−0.008(2)	−0.002(2)
O2	$O_{1.00}$	0.2880(13)	0.7781(7)	0.5697(8)	0.0143(14)	0.027(3)	0.011(2)	0.005(2)	0.005(2)	−0.002(2)	−0.009(2)
O3	$O_{1.00}$	0.9298(12)	0.6136(9)	0.1678(11)	0.021(2)	0.020(3)	0.017(3)	0.022(3)	−0.001(2)	0.012(2)	−0.010(2)
O4	$O_{1.00}$	0.4482(10)	0.9627(7)	0.1217(8)	0.0066(10)						
O5	$O_{1.00}$	0.2821(12)	0.4311(7)	0.5666(8)	0.0136(14)	0.023(3)	0.008(2)	0.004(2)	0.000(2)	−0.003(2)	−0.003(2)
O6	$O_{1.00}$	0.6177(13)	0.6867(9)	0.8167(11)	0.022(2)	0.020(3)	0.022(3)	0.022(3)	0.012(2)	−0.004(3)	−0.005(3)
O7	$O_{1.00}$	0.1681(11)	0.7066(7)	0.8649(9)	0.0117(12)	0.016(2)	0.008(2)	0.013(2)	0.005(2)	0.004(2)	0.002(2)
O8	$O_{1.00}$	0.4489(10)	0.6191(7)	0.1215(8)	0.0088(10)						
O9	$O_{1.00}$	0.9372(13)	0.0003(9)	0.1732(10)	0.0194(15)	0.019(3)	0.025(3)	0.023(3)	0.015(2)	0.010(2)	0.007(2)

Table 6. Selected interatomic distances (in Å) for mambertiite.

Bi	–O1	2.202(6)	Mo1	–O9	1.724(8)	Mo2	–O3	1.711(8)
	–O4	2.236(6)		–O2	1.747(6)		–O5	1.739(6)
	–O8	2.252(6)		–O7	1.901(7)		–O8	1.937(6)
	–O1	2.324(6)		–O4	1.947(6)		–O7	1.943(6)
	–O2	2.476(7)		–O4	2.127(6)		–O8	2.141(6)
	–O9	2.702(8)		–O6	2.584(8)		–O6	2.544(8)
	–O3	2.746(7)		average	2.005		average	2.002
	–O7	2.885(6)						
	average	2.478						
Mo3	–O1	2.031(8)	Mo4	–O6	1.791(9)	Mo5	–O6	1.758(8)
	–O4	2.134(8)		–O4	2.190(6)		–O8	2.197(7)
	–O8	2.164(9)		–O1	2.289(7)		–O5	2.439(7)
	–O9	2.188(10)		–O2	2.393(7)		–O3	2.482(8)
	–O3	2.206(10)		–O9	2.447(8)		–O5	2.519(8)
	–O6	2.509(8)		–O5	2.459(6)		–O2	2.566(6)
	average	2.205		average	2.261		average	2.327

Table 7. Bond-valence calculation (in valence unit, *vu*) for mambertiite.

Site	O1	O2	O3	O4	O5	O6	O7	O8	O9	Σ (X–O)	Theor.
Bi	0.64, 0.50	0.36	0.21	0.60			0.15	0.58	0.23	3.27	3.00
Mo1		1.43		0.83, 0.51		0.15	0.94		1.52	5.38	5.00
Mo2			1.57		1.46	0.17	0.84	0.85, 0.49		5.38	5.00
Mo3	0.13		0.08	0.10		0.04		0.09	0.09	0.53	1.02
Mo4	0.10	0.07		0.13	0.06	0.38			0.06	0.80	1.50
Mo5		0.05	0.06		0.06, 0.05	0.40		0.12		0.74	1.46
Σ (O–X)	1.37	1.91	1.92	2.17	1.63	1.14	1.93	2.13	1.90		
Species	($O_{0.5}OH_{0.5}$)	O	O	O	O	($O_{0.5}OH_{0.5}$)	O	O	O		
Theor.	2.00	2.00	2.00	2.00	2.00	1.00	2.00	2.00	2.00		

In partially-filled sites, bond-valence contribution of each cation has been weighted according to its occupancy

shorter than those reported in some synthetic compounds (around 2.80 Å; *e.g.*, Shieh *et al.*, 1993). A similar Bi–Mo distance was observed for the partially filled Mo3 site in the crystal structure of gelosaite (Orlandi *et al.*, 2011). The average bond distances of the partially occupied Mo sites are significantly longer than those observed in Mo1 and Mo2 polyhedra (up to ~ 2.33 Å for the Mo5 site), probably as a consequence of their partially vacant nature.

3.2. Bond-valence calculation

The bond-valence sums (BVS) for cations show the oversaturation of the Bi, Mo1, and Mo2 sites. The same oversaturation of the Bi atom has been observed calculating the BVS of the gelosaite specimens (from Su Seinargiu and Kingsgate) studied by Orlandi *et al.* (2011), using their atom coordinates, with BVS ranging from 3.25 valence unit (*vu*) to 3.33 *vu* in the pale blue crystal from Su Seinargiu and the sample from Kingsgate, respectively. On the contrary, the Mo atoms at the Mo1 and Mo2 sites in the crystal structure of gelosaite show BVSs [calculated using the bond parameter for Mo^{6+} given by Brese & O'Keeffe (1991)], in good agreement with the expected value for the yellow crystal from Su Seinargiu (5.95 and 5.96 *vu* for Mo1 and Mo2 sites, respectively). The other two samples of gelosaite show a progressive underbonding of the Mo1 and Mo2 atoms (down to 5.65 *vu* at the Mo2 site in gelosaite from Kingsgate), possibly related to the increasing amount of Mo^{5+} substituting for Mo^{6+}. The three partially occupied Mo3, Mo4, and Mo5 are strongly undersaturated with respect to the expected values. Such undersaturation has been observed also for the partially occupied Mo3 and Mo4 sites of gelosaite and is related to their relatively large <Mo–O> bond distances.

The BVSs of the oxygen atoms show a significant deficit for O1, O5, and O6 atoms, with 1.37, 1.63, and 1.14 *vu*, respectively. O6 and O1 atoms are at 2.894(10) and 2.952(9) Å from the O5 atom, respectively, suggesting the possibility of hydrogen bonds when O5···O6 and O5···O1 do not represent polyhedral edges of the additional Mo sites. By using the relation proposed by Ferraris & Ivaldi (1988), the corresponding bond strength is 0.15 and 0.14 *vu*, respectively. In our opinion, O5 is acceptor of hydrogen bonds and the corresponding site could be occupied by an O^{2-} anion. On the contrary, the low BVSs at O1 and O6 sites suggest mixed (O^{2-},OH^{-}) or pure OH^{-} occupancies. By taking into account an ordered distribution of the additional Mo and calculating the corresponding BVSs of O1 and O6 sites, we could hypothesize that both sites have a mixed

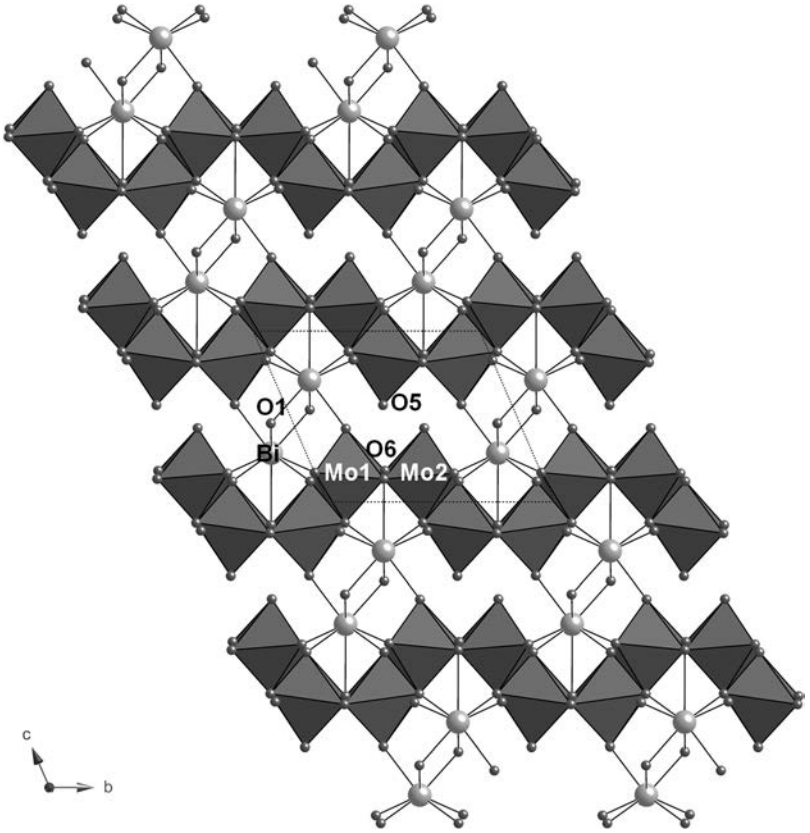

Fig. 3. Crystal structure of mambertiite seen down **a**. Mo1 and Mo2 sites are shown in dark grey; Bi site is shown as grey circles. The position of the O1, O5, and O6 sites are indicated. Partially occupied Mo sites are not shown for sake of clarity.

($O^{2-}_{0.5}OH^{-}_{0.5}$) population. In particular, O1 and O6 would be occupied by an O^{2-} and OH^{-} anion, respectively, when Mo3 is occupied and *vice versa* when Mo5 is occupied. An intermediate situation seems to occur when molybdenum is hosted at the Mo4 site. In addition, it should be stressed that the disordered distribution of the additional Mo could affect the oxygen positions, which are likely only average positions. Consequently, when the additional Mo sites are actually occupied, the oxygen atoms should move to assure shorter Mo–O bond distances; simultaneously, the bond distances with the fully occupied Bi, Mo1, and Mo2 sites should be lengthened. In this way, the BVSs at the Mo3, Mo4, and Mo5 sites would be increased, while the BVS excess at the Bi, Mo1, and Mo2 site would be lowered. This would affect the BVSs of oxygen atoms too.

It is also interesting to compare the BVS of oxygen atoms in mambertiite and gelosaite. The progressive filling of the interstitial Mo sites increases the BVS at the Ow1 site of gelosaite; consequently, whereas an H_2O group occupies this site in gelosaite, a mixed (O^{2-}, OH^{-}) occupancy at this position (corresponding to the O6 site) could be hypothesized in mambertiite. Similarly, the OH^{-} group occupying the OH site in gelosaite could be replaced by a (O^{2-}, OH^{-}) anion in mambertiite at the corresponding site, labelled O1.

4. Discussion

4.1. Structural relationships between mambertiite and gelosaite

The relationships between the crystal structures of mambertiite and gelosaite can be conveniently described on the basis of the OD theory (Dornberger-Schiff, 1964, 1966; Ferraris *et al.*, 2004). Neglecting the additional Mo cations occurring in mambertiite, these two minerals belong to the same OD family. In order to highlight these relationships, the unit cell of gelosaite can be transformed through the matrix [$\bar{1}$ 0 0| 0 $\bar{1}$ 0| 1 0 1]. In this way, the new unit-cell parameters of gelosaite are $a = 5.851$, $b = 9.042$, $c = 14.088$ Å, $\beta = 103.69°$, space group $P2_1/c$.

The single OD layer has translation vectors $\mathbf{a_L}$ and $\mathbf{b_L}$, which are common to mambertiite and gelosaite; the third basic vector $\mathbf{c_0} = \mathbf{c_g}/2$, where $\mathbf{c_g}$ is the unit-cell axis **c** of gelosaite in the standard space group $P2_1/c$, is not a translation vector. The layer symmetry is $P2_1/m$ or, more precisely, $P\,1\,2_1/m$ (1). Adjacent layers may be related by the following operations: a two-fold screw axis parallel to **b**, with translational component **b**/6 ($2_{1/3}$) and a glide reflection perpendicular to **b** with translational component $\mathbf{c}_0$ (c_2). Owing to the

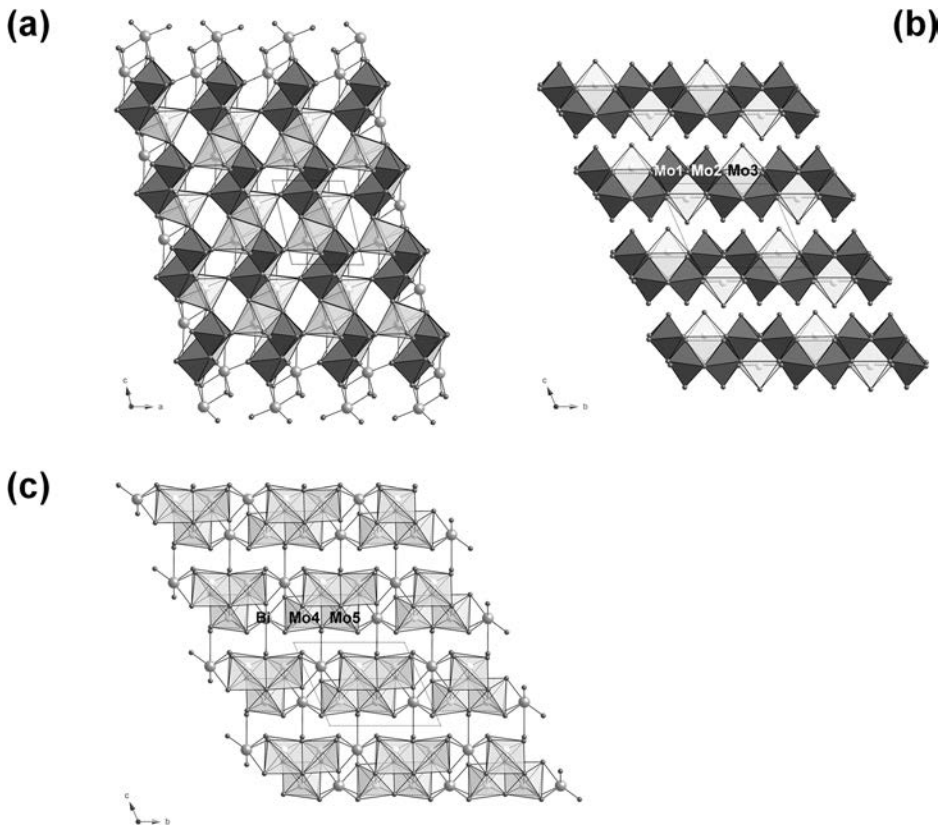

Fig. 4. Crystal structure of mambertiite (a), formed by two kinds of alternating layers: the first one is formed by Mo1, Mo2, and Mo3 site (b), whereas the other is composed by Bi, Mo4, and Mo5 site (c). Dark grey polyhedra = fully occupied Mo sites; light grey = partially occupied Mo sites; ball-and-stick = Bi site; dark grey circles = O sites.

presence of the mirror plane m in the single layer, adjacent layers may be related also through a screw rotation with translational component -**b**/6 ($2_{-1/3}$). Finally, adjacent layers are also related by inversion centres.

The set of λ and σ partial operations (POs) is conveniently represented by the symbol (*i.e.* the ''OD groupoid family symbol''):

$$\begin{array}{llll} P & 1 & 2_1/m & (1) \\ & \{1 & 2_{1/3}/c_2 & (1)\} \end{array}$$

with $a_L = 5.851$, $b_L = 9.042$, $c_0 = 7.044$ Å, $\beta = 103.69°$.

Different sequences of σ POs $2_{1/3}$ and $2_{-1/3}$ give rise to different structures. An infinite number of polytypes, as well as of disordered structures, is possible; in all of them, pairs of adjacent layers are geometrically equivalent. Moreover, in this family two polytypes exist for which not only pairs, but also triples, quadruples... n-tuples of adjacent layers are geometrically equivalent. They are called MDO (Maximum Degree of Order) structures.

If adjacent layers are constantly related by the σ PO [- $2_{1/3}$ -], the λ POs [- 2_1 -] and [- m -] of the single layer are no longer valid for the whole structure. Only the λ and σ inversion centres are total operators. The space group symmetry of this MDO_1 polytype is $P\bar{1}$ (Fig. 5a). The calculated unit-cell parameters are $a = 5.851$, $b = 9.042$, $c = 7.658$ Å, $\alpha = 113.17$, $\beta = 103.69$, $\gamma = 90.0°$, which closely agree with those of mambertiite, *i.e.* $a = 5.854$, $b = 9.050$, $c = 7.637$ Å, $\alpha = 112.85$, $\beta = 102.58$, $\gamma = 90.04°$, space group $P\bar{1}$. The structure obtained when the screw axis [- $2_{-1/3}$ -] is constantly operating is not different from the preceding, corresponding to its twinned {010} counterpart. As a matter of fact, the occurrence of twin-related individuals in crystals of mambertiite has been observed during the single-crystal X-ray diffraction study.

If adjacent layers are related by the σ POs $2_{1/3}$ and $2_{-1/3}$, regularly alternating, the first and the third layers are at the same level and the λ PO 2_1 becomes a total symmetry operator. Moreover, the glide operation c_2 is continued, becoming a true c (c_1) glide, perpendicular to **b**, valid for the whole structure, which has a parameter $c = 2c_0$. The λ PO m is not valid for the whole structure, whereas the λ inversion centres are total symmetry operators. Consequently, the MDO_2 structure has space group symmetry $P\ 1\ 2_1/c\ 1$ (Fig. 5b), with unit-cell parameters corresponding to those of gelosaite transformed in the standard space-group symmetry.

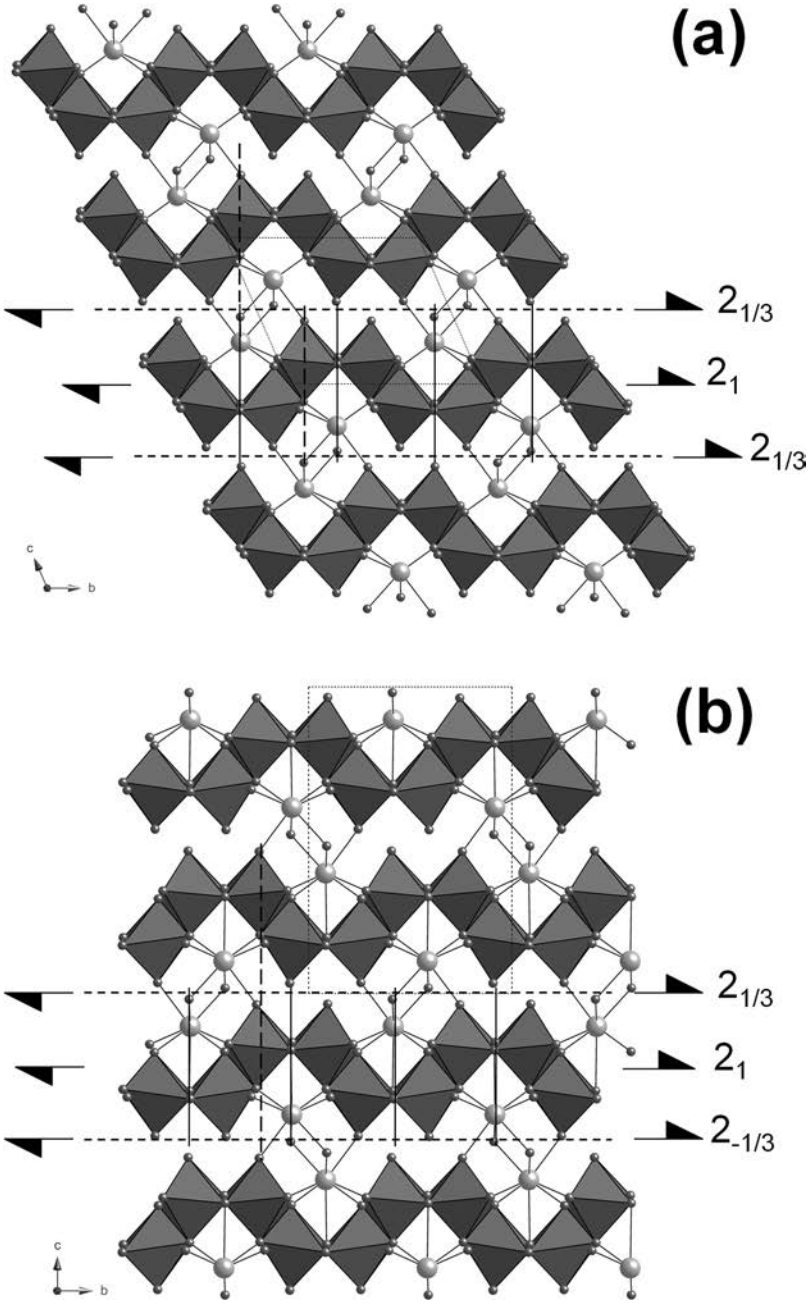

Fig. 5. Crystal structures of the two MDO polytypes of the mambertiite – gelosaite series, as seen down **a**: MDO_1 (a) and MDO_2 (b). Partially-filled Mo sites are not shown.

4.2. Chemical variability in the mambertiite – gelosaite pair

As described in the previous paragraph, from a structural point of view mambertiite and gelosaite show polytypic relationships, being characterized by an 1*A* and 2*M* stacking, respectively. Actually, these two compounds are not true polytypes, owing to their different chemistry related to the occurrence of differently populated Mo3, Mo4, and Mo5 sites.

Orlandi *et al.* (2011) pointed out the presence of only two partially occupied interstitial Mo sites in gelosaite. However, it is important to stress that the final difference-Fourier map of gelosaite from Kingsgate, characterized by the highest content of Mo (2.40 *apfu*), showed an additional small peak that could be attributed to a third fractionally occupied Mo site. Consequently, we may hypothesize the existence of a series between $BiMo^{6+}{}_2O_7(OH) \cdot H_2O$ and a hypothetical compound $BiMo^{5+}{}_3O_9$. The chemical composition of this series can

Table 8. Site occupancies of interstitial Mo sites in gelosaite (in *apfu*) and bond-valence sums (in *vu*) for anions.

	Su Seinargiu (pale yellow)	Su Seinargiu (pale blue)	Kingsgate
Mo3 s.o.f.	0.03	0.06	0.12
Mo4 s.o.f.	0.07	0.13	0.27
Ow1	0.45	0.57	0.83
O2	1.66	1.60	1.63
O3	1.99	2.02	2.04
O4	2.08	2.05	2.05
O5	1.97	1.91	1.92
OH	1.22	1.24	1.31
O7	2.03	2.03	2.02
O8	2.14	2.15	2.30
O9	1.95	1.96	1.90

be idealized as $BiMo_xO_9H_y$. Its variability involves (*i*) the Mo oxidation state, which may be between 6+ and 5+, (*ii*) the Mo cation content, ranging from 2.0 and 3.0 *apfu*, and (*iii*) the H content, required for charge balance, passing from 3 to 0 *apfu*.

The increasing amount of interstitial Mo tends to increase the bond valence sums of the O atoms. Consequently, an inverse relationship between Mo and H contents can be hypothesized: the higher the Mo content, the lower the H content. By calculating the BVS for the crystal structure of the three gelosaite samples studied by Orlandi *et al.* (2011), a progressive increase of the BVS at the Ow1 and OH sites can be observed (Table 8). The BVS increases particularly at the Ow1 site, allowing to hypothesize a mixed occupancy by (OH^-, H_2O), or by OH^- only, in gelosaite from Kingsgate. Consequently, its chemical formula could be $Bi_{1.00}(Mo^{5+}{}_{1.40}Mo^{6+}{}_{1.00})_{\Sigma=2.40}O_7(OH)_2$ and not $Bi_{1.00}Mo^{5+}{}_{2.40}O_7(OH) \cdot H_2O$. The coexistence of Mo^{5+} and Mo^{6+} in this sample could justify its blue colour. In fact, according to Orlandi *et al.* (2011), the blue colour in gelosaite may be related to charge transfer between Mo^{6+} and Mo^{5+} atoms. The pale yellow colour shown by the sample of gelosaite from Su Seinargiu close to the ideal formula, as well as by mambertiite, could be related to the occurrence of Mo in one oxidation state only, *i.e.* 6+ and 5 +, respectively.

The very limited amount of available crystal-chemical data on the mambertiite–gelosaite pair did not allow a complete knowledge of the actual relationships between the two species. In fact, for example, it is not known if the increasing Mo content stabilizes the triclinic structure rather than the monoclinic one or if a triclinic gelosaite (''gelosaite-1*A*'') as well as a monoclinic mambertiite (''mambertiite-2*M*'') could exist. In addition, mambertiite displays the maximum Mo content so far observed in this series of bismuth-molybdenum oxides, ~ 2.8 *apfu*. Consequently, the proposed ideal formula of mambertiite is $BiMo^{5+}{}_{2.80}O_8(OH)$, even if it cannot be excluded that future research could extend the chemical range of mambertiite up to the end-member composition $BiMo^{5+}{}_3O_9$.

Acknowledgements: We are grateful to the mineral collectors Marzio Mamberti and Domenico Preite for providing us with the first specimens of mambertiite. We wish to thank Prof. Silvia Bruni for having recorded the FTIR spectrum. The manuscript was handled by Sergey V. Krivovichev; the comments of two anonymous reviewers helped us in improving the paper.

References

Bonaccorsi, E. & Orlandi, P. (2010): Tancaite-(Ce), a new molybdate from Italy. *Acta Mineral. Petrogr. Abstr. Ser.* 20th General Meeting of the International Mineralogical Association, 21st–27th August, 2010. Budapest, Hungary, **6**, 494.

Brese, N.E. & O'Keeffe, M. (1991): Bond-valence parameters for solids. *Acta Crystallogr.*, **B47**, 192–197.

Bruker AXS Inc. (2001): SADABS. *Bruker advanced x-ray solutions*, Madison, Wisconsin, USA.

Campostrini, I., Gramaccioli, C.M., Demartin, F. (1999): Orlandiite, $Pb_3Cl_4(SeO_3) \cdot H_2O$, a new mineral species, and associated lead-copper-selenite chloride from the Baccu Locci Mine, Sardinia, Italy. *Can. Mineral.*, **37**, 1493–1498.

Chen, M., Zhou, Z., Hu, S. (2002): Bond valence parameters linearly dependent on the molybdenum oxidation states. *Chinese Sci. Bull.*, **47**, 978–981.

Dornberger-Schiff, K. (1964): Grundzüge einer Theorie der OD Strukturen aus Schichten. *Abh. Deutsch. Akad. Wiss. Berlin, Kl. Chem. Geol. Biol.*, **3**, 106 p.

— (1966): *Lehrgang über OD Strukturen*. Akademie Verlag, Berlin, 64 p.

Ferraris, G. & Ivaldi, G. (1988): Bond valence vs bond length in O · · · O hydrogen bonds. *Acta Crystallogr.*, **B44**, 341–344.

Ferraris, G., Makovicky, E., Merlino, S. (2004): *Crystallography of modular materials*. Oxford University Press, New York, 370 p.

Gemmi, M., Campostrini, I., Demartin, F., Gorelik, T.E., Gramaccioli, C.M. (2012): Structure of the new mineral sarrabusite, $Pb_5CuCl_4(SeO_3)_4$, solved by manual electron-diffraction tomography. *Acta Crystallogr.*, **B68**, 15–23.

Holland, T.J.B. & Redfern, S.A.T. (1997): Unit cell refinement from powder diffraction data: the use of the regression diagnostics. *Mineral. Mag.*, **61**, 65–77.

Kraus, W. & Nolze, G. (1996): POWDER CELL – a program for the representation and manipulation of crystal structures and calculation of the resulting X-ray powder patterns. *J. Appl. Crystallogr.*, **29**, 301–303.

Krivovichev, S.V. (2012): Derivation of bond-valence parameters for some cation-oxygen pairs on the basis of empirical relationships between r_0 and *b*. *Z. Kristallogr.*, **227**, 575–579.

Ledain, S., Leclaire, A., Borel, M.M., Raveau, B. (1997a): A Mo(V) monophosphate with an original tridimensional framework: $Li_2Na(MoO)_2(PO_4)_3$. *J. Solid St. Chem.*, **129**, 298–302.

Ledain, S., Leclaire, A., Borel, M.M., Provost, J., Raveau, B. (1997b): A mixed valent molybdenum monophosphate with a

bidimensional connection of MoO_6 octahedra: $Li_3Mo_3O_5(PO_4)_3$. *J. Solid St. Chem.*, **133**, 391–399.

Lovisato, D. (1908): Rosasite, nuovo minerale della miniera di Rosas (Sulcis, Sardegna). *Rend. Accad. Lincei*, **17**, 723–728.

Lu, S.F., Huang, J.Q., Wu, Q.J., Huang, X.Y., Wu, D.X., Zheng, Y., Yu, R.M. (1999): The synthesis and structural characterization of a novel Bi-Mo double cubane cluster coupled by two bridging oxygen atoms $\{[Mo_3(BiI_3)OS_3(\mu\text{-}OAc)_2(py)_3]_2(\mu\text{-}O)_2\} \cdot 2H_2O$. *Polyhedron*, **18**, 281–287.

Mandarino, J.A. (1979): The Gladstone-Dale relationship. Part III. Some general applications. *Can. Mineral.*, **17**, 71–76.

— (1981): The Gladstone-Dale relationship. Part IV. The compatibility concept and its application. *Can. Mineral.*, **19**, 441–450.

Olmi, F., Santucci, A., Trosti-Ferroni, R. (1995): Sabelliite, a new copper-zinc arsenate-antimonate mineral from Sardinia, Italy. *Eur. J. Mineral.*, **7**, 1325–1330.

Orlandi, P., Pasero, M., Bigi, S. (2010): Sardignaite, a new mineral, the second known bismuth molybdate: description and crystal structure. *Mineral. Petrol.*, **100**, 17–22.

Orlandi, P., Demartin, F., Pasero, M., Leverett, P., Williams, P.A., Hibbs, D.E. (2011): Gelosaite, $BiMo^{6+}{}_{(2\text{-}5x)}Mo^{5+}{}_{6x}O_7(OH) \cdot H_2O$ ($0 \leq x \leq 0.4$), a new mineral from Su Senargiu (CA), Sardinia, Italy, and a second occurrence from Kingsgate, New England, Australia. *Am. Mineral.*, **96**, 268–273.

Orlandi, P., Gelosa, M., Bonacina, E., Caboni, F., Mamberti, M., Tanca, G.A., Vinci, A. (2013): Sardignaite, gelosaite et tancaite-(Ce): trois nouveaux minéraux de Su Seinargiu, Sarroch, Sardaigne, Italie. *Le Regné mineral*, **112**, 39–52.

Orlandi, P., Biagioni, C., Bindi, L., Nestola, F. (2014): Ichnusaite, $Th(MoO_4)_2 \cdot 3H_2O$, the first natural thorium molybdate: occurrence, description, and crystal structure. *Am. Mineral.*, **99**, 2089–2094.

Orlandi, P., Biagioni, C., Bindi, L., Merlino, S. (2015): Nuragheite, $Th(MoO_4)_2 \cdot H_2O$, the second natural thorium molybdate and its relationships to ichnusaite and synthetic $Th(MoO_4)_2$. *Am. Mineral.*, **100**, 267–273.

Passaglia, E. & Pongiluppi, D. (1975): Barrerite, a new natural zeolite. *Mineral. Mag.*, **40**, 208.

Passaglia, E., Galli, E., Leoni, L., Rossi, G. (1978): The crystal chemistry of stilbites and stellerites. *Bull. Minéral.*, **101**, 368–375.

Sheldrick, G.M. (2008): A short history of SHELX. *Acta Crystallogr.*, **A64**, 112–122.

Shieh, M., Mia, F.D., Peng, S.M., Lee, G.H. (1993): Synthesis and X-ray crystal structure of a tetrahedral bismuth-molybdenum carbonyl complex possessing three bridging methoxy ligands, $[Et_4N]_2[BiMo_4(CO)_{12}(\mu_3\text{-}OMe)_3)$. *Inorg. Chem.*, **32**, 2785–2787.

Wilson, A.J.C. Ed. (1992): *International Tables for Crystallography. Volume C: Mathematical, Physical and Chemical tables*. Kluwer Academic, Dordrecht, NL.

Wittich, E. & Neumann, B. (1901): Ein neues Cadmium Mineral. *Central. Mineral. Geol. Paläont.*, **1901**, 549–551.

Received 24 October 2014
Modified version received 31 December 2014
Accepted 7 January 2015